



High-resolution WRF simulations of a monsoon event (2019) over the Badulu Oya Catchment, Sri Lanka: Role of cumulus parameterization condition and microphysics schemes

P G S GIMHAN^{1,*} , PANDUKA NELUWALA¹ and RALPH ALLEN ACIERTO²

¹*Department of Civil Engineering, Faculty of Engineering, University of Peradeniya, Peradeniya 20400, Sri Lanka.*

²*International Center for Water Hazard and Risk Management (ICHARM), 1-6, Minamihara, Tsukuba-shi, Ibaraki-ken 305-8516, Japan.*

*Corresponding author. e-mail: samurdagimhan@gmail.com

MS received 2 February 2023; revised 19 June 2023; accepted 19 July 2023

Numerical weather modelling has piqued the attention of the hydrological community because precise predictions from the models might lessen the extreme hydrological repercussions. Despite the paucity of existing studies, significant tropical storms frequently affect the Asian island of Sri Lanka. This research investigates the Weather Research Forecast (WRF-ARW) model's cumulus parameterization condition and physical parameterization schemes for a 2019 northeast monsoon event over the Badulu Oya Basin, Sri Lanka. Three cumulus schemes (Kain–Fritsch (KF), Betts–Miller–Janjic (BMJ) and Multi-scale Kain–Fritsch (MKF)) and four microphysics schemes (WRF single-moment 5-class (WSM5), WRF single-moment 6-class (WSM6), Kessler (KSL) and WRF double moment 6-class (WDM6)) were evaluated for their impact on modelled rainfall. The model performances were assessed using 24-hr accumulated model rainfall and observed rainfall with various model configurations at a horizontal grid resolution of 3 km using categorical and two quantitative comparison techniques. The study concluded that the activated KF scheme with a finer domain resolution (3 km) would be preferred for cumulus parameterization in the study region. The KF-WSM5 combination was the best since it produced the highest statistics: ETS is 0.38, B is 0.95, r is 0.76, NSD is 1.06, NRMSE is 0.72, and CCPA is 75%.

Keywords. High-resolution WRF-ARW model; northeast monsoon rainfall; Badulu Oya catchment; cumulus condition; microphysics.

1. Introduction

The Indian Ocean possesses robust intraseasonal atmospheric fluctuation, where a boreal summer oscillation can substantially modify the phases of the South Asian monsoon as it propagates towards the Bay of Bengal (Lawrence and Webster 2002;

Bandurathna *et al.* 2021). Sri Lanka, a country adjacent to the Indian subcontinent, is susceptible to dramatic shifts in rainfall due to the advent of low-pressure systems that trigger pressure gradients in the Bay of Bengal. These fluctuations develop into intense tropical storms across the island during the early phase of the northeast

monsoon and the late phase of the southwest monsoon (Perera *et al.* 2017; Rajapaksha *et al.* 2020; Ruwangika *et al.* 2020). The northeast monsoon is prevalent from December to March, whereas the southwest monsoon is prevalent from May to September. These storms typically create significant flooding and landslides around the nation, drowning entire areas and damaging dwellings. Therefore, accurate forecasting of severe precipitation episodes at various temporal scales has substantial scientific and economic ramifications.

In Sri Lanka, monsoon-induced heavy precipitation events have not received much attention from various perspectives or numerical weather prediction models (NWP) over the previous few years. Darshika and Premalal (2015) applied the Weather Research and Forecasting (WRF) model to examine rainfall events associated with the 2014 northeast monsoon across Sri Lanka at a 30 km lower resolution. They concluded that Kessler and Kain–Fritsch, WSM5 and Kain–Fritsch, WSM6 and Betts–Miller–Janjic were able to forecast observed rainfall patterns across the island's northeastern coastline regions and in the interior areas next to the coast as microphysics and cumulus parameterization, but those combinations were failed to record the distribution of rainfall anywhere else on the island. Another WRF model investigation was conducted by Nandalal *et al.* (2012), who examined rainfall episodes associated with the 2008 and 2009 at a 5 km resolution. The investigation concluded that the Ferrier microphysics and Kain–Fritsch cumulus schemes yielded good rainfall forecasts for the Nilwala river basin. Muhammadh *et al.* (2017) attempted to replicate two monsoon rainfall events in Sri Lanka over the Upper Mahaweli basin using the RegCM model by selecting appropriate physics options with a 10 km resolution and arrived at the conclusion that the Emanuel cumulus convection scheme (Emanuel 1991) in the RegCM model is the finest. Bandurathna *et al.* (2021) evaluated the forecasting ability of existing dynamic models for modelling the southwest monsoon by leveraging ECMWF simulation data from the S2S project (subseasonal to seasonal prediction project of the World Weather Research Program/World Climate Research Program) over Sri Lanka. The results of the experiment revealed that the wind index is more accurately predicted by the ECMWF (European Centre for Medium-Range Weather Forecasts) model than the rainfall index. Because

all of these studies are primarily concerned with establishing the optimal physics scheme combination to simulate the observed monsoon precipitation events, little is known regarding performance when the cumulus physics scheme (CPS) is turned off within the finer domain resolution.

The CPS in NWP) indicates the influence of convection on environmental variables, whereas a microphysics scheme (MPS) describes precipitation with grid-resolved variables (Kwon and Hong 2017). Earlier studies have shown that NWP) precipitation predictions are directly influenced by the CPSs and MPSs, while the precipitation simulation is less dependent on MPS than the CPS (Nasrollahi *et al.* 2012; Chawla *et al.* 2018; Liu *et al.* 2018). CPS is crucial for controlling the amount of water vapour present in a computational model that simulates latent heat discharges and vertical fluxes (Arakawa 2004). Heat is released from condensation in convective processes when atmospheric motion is combined, providing a credible explanation for observations (Zhang *et al.* 1998; Donner *et al.* 2001). The CPSs are multiplied by their numerous intricate subgrid flux parameterizations (Kwon and Hong 2017). The moisture convergence type, adjustment type and mass-flux type are the three leading CPS classes (Kwon and Hong 2017). The two primary objectives of dramatically extended CPSs are to locate mass-specific vertical integration of cumulus heating and to acquire vertical scatterings of cumulus amounts (heating and drying amounts) (Kuo 1974; Arakawa 2004).

The leading assumption while making the medium-range forecasts using the Global Climate Models (GCMs) is that the amount of upflow clouds is minimal compared in relation to the grid box in the model. In the context of climate communities, this supposition applies to GCMs with a grid size greater than 10 km, but it is erroneous for grid resolution of less than 5 km (Kwon and Hong 2017). Many investigations on the MPSs of regional models with horizontal grid spacing under 5 km have been performed, omitting CPSs, which are assumed to be a scale for resolving clouds (Bryan and Morrison 2012; Schwartz and Liu 2014; McMillen and Steenburgh 2015). All the conducted studies are unable to reach the best conclusion even when the CPSs are disregarded because grid-scale impact at the tested resolution, which is less than 5 km, does not adequately resolve the precipitating convection (Clark *et al.* 2012). The 'gray zone' effect refers to this phenomenon and beyond the

upper bound of model horizontal grid spacing, which is in the 2–10 km range. To assess if a CPS is best for their horizontal grid scale, users must either disregard the scale altogether or conduct straightforward testing (Hong and Dudhia 2012; On *et al.* 2018). Even though no CPS is utilised in the high-resolution inner domains, the effects of the CPS may spread from the outer domain to the high-resolution inner grids across the borders in NWP (Li *et al.* 2018). Given these facts, the employment of cumulus parameterization schemes, frequently with model grid resolutions below 10 km, is still controversial (Li *et al.* 2018).

The MPS, regarded as more robust than the CPS, is activated when the average relative humidity in grid cells is more than 100%. Water vapour, cloud droplets, graupel, raindrops, snow and hail are significant species on a microscopic scale, and the segregation of these species is determined by the characteristics of atmospheric dynamics and thermodynamics (Huang and Wang 2017). Most MPSs contain two or three ice categories used in NWP and climate models. The significance of microphysical processes in forecasting precipitation from thunderstorms and synoptic scale convective systems has been underlined in numerous studies (De Meij *et al.* 2018; Maheskumar *et al.* 2018). Incorporating microphysics of clouds with a mixed ice–water phase into the NWP model improves convection model outcomes notably and becomes more significant for rainfall situations linked to surface cyclone systems connected to monsoonal precipitation (Lim and Hong 2005). According to Huang *et al.* (2016), the distribution of large-scale vertical motion was closely related to the fluctuation of precipitation intensity with MPSs.

Regional Climate Models (RCMs) are strenuously focused on reflecting the regional characteristics rather than the global conditions that are dynamically combined to GCMs for overcoming the GCM constraints (Mukhopadhyay *et al.* 2010; Yang *et al.* 2012; Ji *et al.* 2013; Bliznak *et al.* 2019). One of the most prominent RCMs for simulating or forecasting regional weather and climate at a reasonably high resolution is the WRF model (Avolio and Federico 2018; Hasan and Islam 2018; Skamarock *et al.* 2019; Scaff *et al.* 2020). Advanced Research WRF (ARW) dynamical core within the WRF model is extensively utilised in regional climate research with fine tweaking its inherent physics schemes: microphysics scheme (MPS), cumulus physics scheme (CPS), surface layer scheme, planetary boundary layer scheme, land

surface scheme, short wave radiation scheme and long wave radiation scheme (Kumar *et al.* 2008; Dudhia 2014; Dasari and Salgado 2015; Skamarock *et al.* 2019). Previous research has revealed that the Penn State/NCAR Mesoscale Model 5 (MM5) has lesser simulation capabilities than the WRF-ARW model (Bruno *et al.* 2014; Lee *et al.* 2015; Tian *et al.* 2017).

This study's primary goal is to analyse any ambiguity regarding the suitability of CPSs for fine resolution. A number of WRF-ARW model simulations were executed to assess the results of using and not using a CPS (Kain–Fritsch (KF), Betts–Miller–Janjic (BMJ) and Multi-scale Kain–Fritsch (MKF)) within the innermost nest (3 km). An actual rainfall event in December 2019 was emulated to assess how effectively the tested model combinations performed in correctly predicting the spatial distribution of daily accumulated rainfall across the Badulu Oya basin. An inter-comparison was performed at one-by-one rainfall stations using model results and recorded precipitation daily data for the selected northeast monsoon rainfall event over the catchment. Reliability of the amount and position location of the rainfall was evaluated using categorical and two quantitative comparison techniques, which involved correlating the modelled 24-hr precipitation result to the real 24-hr precipitation quantities. The research methodology, including the study location, precipitation event of interest, model configuration, design of experiments, data and result comparison methodologies utilised for the tested event, are presented in section 2 of this article. After an overview of the findings in section 3, general conclusions are presented in section 4.

2. Materials and procedures

2.1 Study area and extreme precipitation event in December 2019

Sri Lanka is a country in South Asia situated in the main Indian Ocean Sea lanes within a latitude range of 5°55'–9°51'N and a longitude range of 79°42'–81°53'E. The Badulu Oya watershed is a key sub-catchment of the upper Mahaweli drainage basin, covering an area of 404 km² inside the district of Badulla (figure 1). The Badulu Oya travels 59 km across the country's central highlands before joining the Mahaweli River, Sri Lanka's largest river. The catchment receives between 1500 and

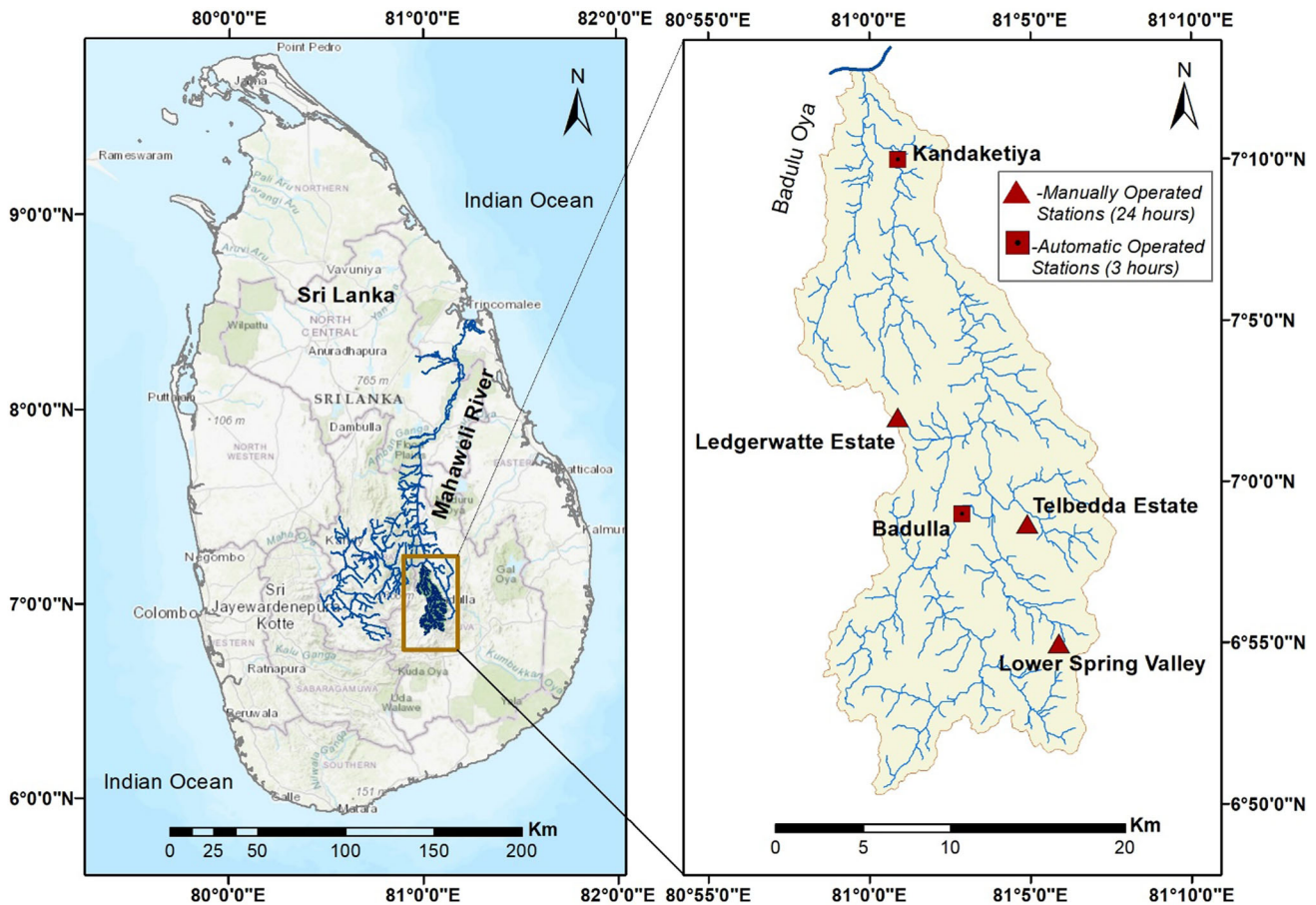


Figure 1. Badulu Oya catchment including locations of the selected rainfall gauges.

2000 mm of rain each year (Atukorala 2012; Ruwangika *et al.* 2020). High showers in the Badulla area result from the northeast monsoon, which is characterised by a predominance of mesoscale characteristics over synoptic features due to poor wind stream on the northeast side and a poor significant pressure variation. The extreme rainfall events often trigger massive landslides on the steep farmlands within the Badulu Oya region. This typically occurs whenever there is 75–100 mm of continuous rain over two days (Perera *et al.* 2017).

The Badulu Oya watershed received high precipitation in numerous areas in December 2019. During the first week of December 2019, the Indian Ocean Dipole was significantly positive (>2), and the Madden–Julian Oscillation (MJO) was in phases 2–3, which were favourable for the development of northeast monsoonal storms in Sri Lanka (Balachandran *et al.* 2020). The northeast monsoon produced a severe rainfall event from December 1–8, 2019, with the daily maximum rainfall amount of 130 mm reported in the Lower

Spring Valley area within the Badulu Oya catchment on December 4, 2019 (Ministry of Defense 2019; DMSL 2020). A total of 14,164 people (4153 families) across 14 districts, including the Badulla area, were impacted by the rainfall event. Since November 30th, 2019, one person has been reported missing, and five deaths have been reported. Severe storms and landslides caused 259 houses to be slightly destroyed, six houses to be completely destroyed, and 3149 people from 946 families to be shifted into one of the 29 sites put up throughout numerous districts, including the Badulla area, to support those who were affected (Government of Sri Lanka World Food Programme 2019). Many main roadways in Badulla and the surrounding regions were impassable due to earth slips and inundations caused by the extremely heavy rainfall (Staff Writer 2019).

2.2 WRF model and experimental design

The National Center for Atmospheric Research's (NCAR) WRF model, version 4.1.3, was utilised

for the simulations. The WRF-ARW dynamical core model includes physics options such as radiation schemes, boundary layer options, and cumulus schemes, which also has the potential to support several nesting. Available physics choices of parameterization schemes differ in complexity, effectiveness, applicability, and computing expense cost (Skamarock *et al.* 2019; National Center for Atmospheric Research 2020). Only the microphysics and cumulus schemes were altered for the present investigation, while the other schemes remained unchanged, and the same scheme was introduced into all domains for the particular model experiment in order to attempt to reduce discrepancies at the processing grid interface (Warner *et al.* 1997). Table 1 lists the WRF-ARW model options utilised in this investigation. This study used a two-way nested domain configuration due to its better precipitation prediction ability compared to a one-way nesting setup. This is attributed to the absence of inconsistency between the outcomes of parent and nested grids. In this setup, wherever the coarse and nested grids overlap, there is an interaction between the two, and the solution on the coarse grid depends on the nested grid (Madhulatha *et al.* 2021). This research evaluated the daily accumulated rainfall as of 0600 UTC on each day over a span of 7 days. This model start time (0600 UTC) was selected so as to

account for minor temporal variations of the filed recording time in the 24-hr rainfall data provided by the Department of Meteorology in Sri Lanka (DMSL).

Lateral boundary and starting conditions from the GCMs are mandatory for the WRF-ARW model to run as a high-resolution area-specific model (Skamarock *et al.* 2019). For preliminary and lateral constraints, 1-degree by 1-degree grids with high-resolution NCEP (National Centers for Environmental Prediction) Final Analysis (GFS-FNL) produced at 6-hr intervals were utilised (National Center for Atmospheric Research 2019). The outer domain received the preliminary and lateral constraints during the model simulations, which resulted in the necessary boundary constraints for the inner domains. The most widely utilised terrestrial dataset in WRF studies was provided through the WRF users' website (National Center for Atmospheric Research 2020), which was inserted as the model's input terrestrial data here.

2.3 Cumulus and microphysical parameterization sets

For the investigation, three CPSs and four MPSs were chosen with enough variation in the treatment of ice particles, parameter distribution and

Table 1. Modelling selections in this research.

Variables	Selected alternative	Citations/comments
Software	WRF-version 4.1.3	(National Center for Atmospheric Research 2020; Skamarock <i>et al.</i> 2019); Advanced Research WRF (ARW) dynamical core was engaged
Domains	27 km (D1)/9 km (D2)/3 km (D3)	100 × 100, 100 × 100 and 34 × 34 were selected for horizontal and vertical grid points, see figure 2
Time step	100 seconds	A ratio of 3:1 was used for nests
Modelling duration	Start: 0600 UTC (Coordinated Universal Time) on 01 December 2019 End: 0600 UTC on 09 December 2019	8 days; first 24 hours (first day) considered as the spin-up period and each day within remaining 7 days were investigated
Planetary boundary layer	Yonsei University scheme (YUS)	(Hong <i>et al.</i> 2006); effectively applied to real-time convective predictions
Long wave radiation	The Rapid Radioactive Transfer Model (RRTM)	(Mlawer <i>et al.</i> 1997); represent subgrid scale radiative processes
Short wave radiation	Dudhia scheme	(Dudhia 1989); effect of solar zenith angle was taken into account
Land surface	Unified Noah scheme	(Mukul Tewari <i>et al.</i> 2004); surface heat fluxes compared favorably with observations
Surface layer	Revised MM5 scheme	(Jimenez <i>et al.</i> 2012); proper represents the land surface properties

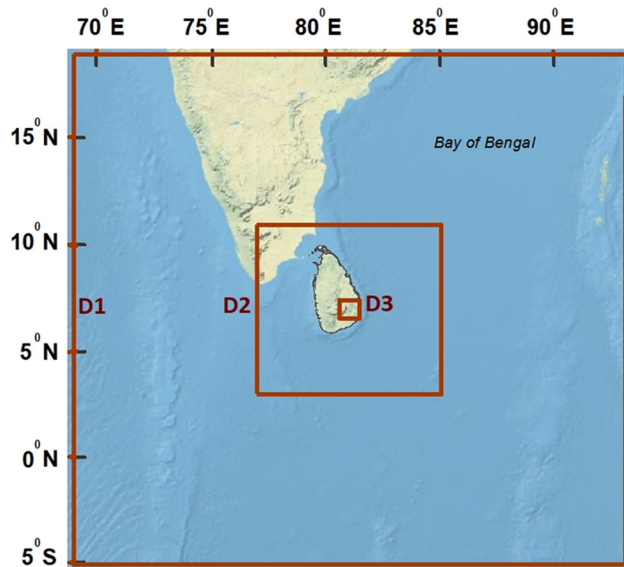


Figure 2. WRF domain configuration with grid resolutions of 27 km (D1)/9 km (D2)/3 km (D3).

complexity between them. Every experiment combines a CPS with an MPS while activating cumulus parameterization for every domain despite the resolution. Numerous comparative studies to examine the effects of using (or not using) the various schemes could not be performed due to computer capabilities and time framework. On the basis of their performance in previous studies, five model combinations relating to the identified CPSs and MPSs were evaluated (Kumar *et al.* 2008; Nandalal *et al.* 2012; Darshika and Premalal 2015; Chawla *et al.* 2018; De Meij *et al.* 2018; Rodrigo *et al.* 2018; Singh *et al.* 2018; Samarasingha *et al.* 2021). Only the inner grid's output meteorological data was evaluated in this research study. The inner grid lies within the gray zone grid scale limit, where it is uncertain whether to use the cumulus scheme (Hong and Dudhia 2012; On *et al.* 2018). Given this information, a simulation with explicit cumulus formation at a 3-km resolution (D3) and the activation of CPS in the outer domains (D1 and D2) was included in this investigation to examine the relationship between precipitation and the status of the CPS. This research consists of ten trials: five with the chosen CPSs and MPSs and five with the CPS turned off in the inner domain of the same specified combinations.

2.3.1 A simple overview of selected cumulus schemes

The three CPSs that are the focus of this study are the following:

- (a) The Kain–Fritsch (KF) scheme is a vertical momentum dynamic with Lagrangian parcel approach-based mass-flux type parameterization scheme. Generally, it can be divided into three sections: the mass flux generation, the convective trigger mechanism, and the closure presuppositions. These sections can describe sub-grid scale characteristics of updraft and downdraft processes that produce intense convection. The small-scale processes that result in convection can be explained by this model (Kain 2004).
- (b) The thermally-generated turbulent mixing in convection is included in the Betts–Miller–Janjic (BMJ) convective adjustment scheme. An empirically derived quasi-equilibrium thermodynamic profile is employed in place of a wet adiabat as the reference state for the deep convection. Deep convection has more consistent temperature profiles, while the moisture profiles vary more between equilibrium states (Vaidya and Singh 2000). According to Vaidya and Singh (2000), the BMJ scheme suppresses the erroneous distribution of rainfall in the Arabian Sea and the Bay of Bengal.
- (c) The Multi-scale Kain–Fritsch (MKF) scheme is an improved version of the Kain–Fritsch (KF) scheme that accounts for the lifting condensation level-based entrainment and the subgrid-resolution effect of cloud radiation reactions with the cloud updraft mass fluxes. With the intention of obtaining climate predictions at grid spacings ranging from 3 to 9 km, these modifications establish scale dependency for several of these essential KF scheme elements (Zheng *et al.* 2016).

2.3.2 A simple overview of selected microphysics schemes

An overview of the selected MPSs is presented below:

- (a) The basic WRF single-moment 3-class (WSM3) scheme provided development to the WRF single-moment 5-class (WSM5) microphysics scheme. The mixed phase WSM5 incorporates five different species of water (snow, ice, cloud, rain, and vapour) as prognostic water substance variables (Hong and Lim 2006). According to Hong and Lim (2006),

the amount of rainfall increases as the number of hydrometers increases for higher resolutions. Additionally, their research stated that cloud ice accumulation is a crucial element for improving the simulation of monsoonal heavy rainfall and large-scale in the eastern part of Asia.

- (b) Another predictive variable introduced to the WSM5 in the WRF single-moment 6-class (WSM6) scheme is the grain (six water species). The representations of the ice cloud attributes in these schemes are more accurate when cloud radiation feedback is accounted. In terms of upper-level mean temperature, the ice cloud significantly impacts longwave heating more than shortwave heating (Hong and Lim 2006).
- (c) The Kessler (KSL) scheme is the most established microphysics scheme utilised by the WRF model. This liquid-only scheme incorporates rain, cloud water and water vapour. The primary processes in this scheme are the production, fall, and evaporation of rain, the accretion and auto-conversion of cloud water and the production of cloud water from condensation (Mielikainen *et al.* 2013).
- (d) The WRF double moment 6-class (WDM6) system can account for the aerosol effect of clouds by taking into account both the mass and concentration of cloud droplets. The WDM6 scheme is an upgraded version of the WRF single-moment 6-class microphysics scheme (WSM6) that takes into account the number of concentrations of cloud droplets and rain. This scheme is superior to other double-moment microphysics schemes because it accounts for radar reflection (Lim and Hong 2010).

In the following sections, each experiment will be referred to as a combination of the ‘Cumulus-Microphysics’ options; for example, the experiment that combined Kain–Fritsch cumulus scheme with the WRF single-moment 5-class microphysics scheme will be referred as ‘KF-WSM5’. Five combinations: (i) KF-WSM5, (ii) KF-WSM6, (iii) BMJ-KSL, (iv) MKF-WDM6 and (v) MKF-WSM6 were selected to assess the model performances. The MPS solves for total precipitation when a CPS is disabled inside the innermost domain (D3). When this occurs, the combination is known as ‘Off-Cumulus-Microphysics’. For instance, ‘Off-KF-WSM5’ refers to an experiment that combines

Kain–Fritsch cumulus scheme with the WRF single-moment 5-class microphysics scheme and disables the CPS (KF) within the innermost domain (D3).

2.4 Observation data and verification methods for WRF simulations

Surface observations provided by DMSL stations in Kandaketiya, Ledgerwatte Estate, Badulla, Telbedda Estate and Lower Spring Valley were utilised to compare precipitation variables during the examined duration of the event. The coordinates for these five selected rain gauges are (7°10′0.00″N, 81°1′0.00″E), (7°1′60.00″N, 81°1′0.00″E), (6°58′60.00″N, 81°2′60.00″E), (6°58′42.00″N, 81°5′2.00″E) and (6°55′0.00″N, 81°5′60.00″E) as shown in figure 1. Badulla and Kandaketiya are the only stations of their type that have an automatic recording period of 3 hours. The remaining manually operated stations have a precision of up to 0.1 mm. Daily rainfall totals from these particular gauges were used to evaluate the performance of the tested models. The model simulations’ inner domain (see figure 2) is where all comparisons are made. In the WRF model, precipitation can be generated explicitly using the MPS (i.e., implicit precipitation) or implicitly using the CPS (i.e., explicit precipitation). This study defined total precipitation as the sum of these two types. The amount and location of rainfall were examined using a categorical (2×2 contingency table) and two quantitative comparison techniques (normalised Taylor diagram and spatiotemporal analysis), which involved correlating the predicted 24-hr precipitation result to the observed 24-hr precipitation quantities at each surface rain gauge station.

2.4.1 2×2 Contingency table

The 2×2 cross-tabulation approach is extensively employed in the statistical evaluation of predicted and observed data in the categorical evaluation. The accumulated daily rainfall of the selected five rainfall stations over a seven-day period, which contributed a total of 35 data pairs, was examined for this evaluation. Threshold values for cumulative rainfall of 1, 2, 5, 10, 25, and 50 mm/day are commonly inferred for many documented categorisation computation techniques in the literature, with higher limits suggested if high-value events have been recorded (Brown *et al.* 2004). As

a result, this study assessed the 35 data pairings using 10, 25, and 50 mm/day thresholds that have more than five occurrences in the dataset, with higher threshold limits equivalent to a substantially regarded heavy precipitation event. The proportion correct (PC), probability of detection (POD), and false alarm ratio (FAR) were calculated separately under three threshold limits (Wilks 2011). The bias (B) and equitable threat score (ETS) were calculated separately for three threshold limits and averaged to acquire an overall view of the model performance (Wilks 2011). The proportion of accurate projections is calculated by PC and is influenced by both correct rejections and hits. The PC can be between 0 and 1, with 1 being the highest possible score. The POD, where 1 is the best possible score, is derived by comparing the percentage of observed precipitation that the model correctly predicted and has a range of 0 to 1. It is susceptible to the intensity of precipitation that occurs throughout the event. FAR measures the percentage of the predicted rainfall that did not happen. This index disregards ‘misses’ and considers how frequently rain fell during the event. The bias (B), where the optimum value is 1, and the value can range from 0 to infinity, determines how WRF simulated precipitation at more or fewer stations than what was really recorded. The ETS (Gilbert Skill Score) compares two sets of data and applies the correction term for a successful simulation caused by probability-driven simulation success, with 1 being the best performance and 0 representing the same accuracy of the compared data. The average values of ETS and B across the three rainfall thresholds were utilised to succinctly summarise the model’s performance in forecasting rainfall. Below are the equations (1–5) for these categories’ indices:

$$PC = \frac{YY + NN}{n} \quad (1)$$

$$POD = \frac{YY}{YY + NY} \quad (2)$$

$$FAR = \frac{YN}{YY + YN} \quad (3)$$

$$B = \frac{YY + YN}{YY + NY} \quad (4)$$

$$ETS = \frac{YY - \frac{(YY+YN)(YY+NY)}{n}}{YY + YN + NY - \frac{(YY+YN)(YY+NY)}{n}} \quad (5)$$

The n possible combinations of modeled and observed precipitation data with a rain/no-rain scenario were compared using a 2×2 contingency table to calculate the aforementioned indices. The YY implies correct predictions that resulted in precipitation (hits), the YN indicates correct predictions that resulted in no precipitation being recorded (false alarms), the NY denotes incorrect predictions that resulted in precipitation being recorded (misses), and the NN indicates incorrect predictions that resulted in no precipitation being either predicted or recorded (correct rejections).

2.4.2 Normalised Taylor diagram

Precipitation forecasts can be examined directly by comparing them to observed data and computing several statistical measures, such as standard deviation, correlation coefficient, bias, and root mean square error. Integrating a wide range of variables with a variety of different units, normalised Taylor diagrams graphically display measures of correlation and standard deviation (NCAR 2019). NSD (normalised standard deviation), r (correlation coefficient), bias error (Bias), and NRMSE (normalised root mean square error) were calculated using the accumulated daily rainfall of the selected five rainfall stations over a seven-day period, yielding a total of 35 data pairs (see equations 6–9 below).

$$NSD = \frac{\sigma_f}{\sigma_r} \quad (6)$$

$$r = \frac{\frac{1}{N} \sum_{i=1}^N (f_i - \underline{f})(r_i - \underline{r})}{\sigma_f \sigma_r} \quad (7)$$

$$Bias = \frac{(\underline{f} - \underline{r})}{\underline{r}} \quad (8)$$

$$NRMSE = \frac{\sqrt{\frac{\sum_{i=1}^N (r_i - f_i)^2}{N}}}{\sigma_r} \quad (9)$$

where f_i stands for forecast cumulative precipitation values of the models, r_i for reference (observed) precipitation values, which are defined at N discrete points (in time and space). \underline{f} and \underline{r} are the area-averaged mean values and σ_f and σ_r are the standard deviations of f and r , respectively. Normalised Taylor diagrams were used to visually portray these statistics after reviewing the NCAR website’s technical specifications (NCAR 2019). WRF models that match reference accurately will

be located closest to the x-axis point in the diagram labelled ‘REF’. These WRF models will have modestly low NRMSE, a fair amount of correlation and the correct amplitude of variation (NSD). A smaller bias score also indicates that the predictions are reasonably close to the data.

2.4.3 Spatiotemporal analysis

The ArcGIS software with the inverse distance weighting (IDW) technique tool was utilised to compare the spatiotemporal distribution of predicted WRF rainfall data to rainfall gauge data within 3 km × 3 km (44 grid boxes) on the maximum daily rainfall recorded day. The IDW approach employs an interpolation process in which the influence of one point in relation to another decreases as the distance from the grid node increases by assigning weights to data points with a weighting power (Lu *et al.* 2008). In the present investigation, a power of two with a 3 km output grid size, a variable search radius, the observed values from five rainfall gauge stations as input data, 44 cell points as output locations, and the entire Badulu Oya catchment as a barrier were utilised. The observed precipitation values for the day with the highest total rainfall were computed using the IDW interpolation method at the midpoint of each of the 44 grid units. Finally, 44 observed values at the same grid points were compared to the WRF output data. The Mean Absolute Model Error Percentage (MAME; see equation (10) below) was used to visualise the difference between daily rainfall that was predicted and observed (Samarasingha *et al.* 2021).

$$\text{MAME} = \frac{(f_i - r_i)}{r} \times 100 \quad (10)$$

where f_i denotes the model’s predicted cumulative precipitation values, and r_i is the reference (recorded) precipitation values defined at the grid points. r is the area averaged mean value of r . Grid-wise correctly predicted area (GCPA), which was determined between –50% and 50% of MAME, was utilised to evaluate the overall competency of the models that were tested.

3. Results and discussions

According to the Thiessen polygon approach, the acquired area-averaged precipitation values for the modelled event are in figure 3 for the five

rainfall stations inside the study area. This technique involves the construction of polygons that perpendicularly intersect the midpoint of the connecting line between two rain stations in the study area. Subsequently, the area-averaged rainfall value of five stations on a particular day is calculated by computing the product of each polygon’s area and the corresponding rainfall value of the station located within the polygon, and dividing the sum of these products by the total area (Arianti *et al.* 2018). Combinations of the KF-WSM5, KF-WSM6, Off-KF-WSM6, MKF-WDM6, Off-MKF-WDM6 and MKF-WSM6 follow the pattern of the area-averaged observed value plot. Although the area-averaged forecasted maximum rainfall amounts did not match the area-averaged observed peak (86.4 mm/day) on December 4, 2019, KF-WSM5, KF-WSM6, Off-KF-WSM6, MKF-WDM6, MKF-WSM6 and Off-MKF-WSM6 were able to capture the peak.

As explained in the previous section, three methods are used to evaluate the model’s 24-hourly cumulative precipitation at the five observational stations that collected 24-hourly gauge precipitation data. The results of these methods are indicated below.

3.1 Categorical verification method comparison – 2 × 2 contingency table

Figure 4 depicts the pertinent findings for the 2 × 2 contingency table analysis. Off-BMJ-KSL achieves the greatest PC value (0.83) at the 25 mm limit, whereas Off-MKF-WSM6 achieves the best PC value (0.83) at the 10 mm bound. At the 50 mm limit, KF-WSM5, Off-KF-WSM6, and MKF-WDM6 had the most significant PC values (0.94). MKF-WSM6 has the maximum POD value in both the 10 mm (0.96) and 25 mm (1.00) limits. In the 50 mm limit, POD values of 1.00 are observed for BMJ-KSL, Off-BMJ-KSL, MKF-WSM6, and Off-MKF-WSM6. Off-MKF-WSM6 achieves the best FAR in the 10 mm limit (0.06). In 25 and 50 mm limits, Off-KF-WSM5 and Off-KF-WSM6 have zero FAR values, respectively. The FAR value relevant to Off-KF-WSM5 in the 50 mm threshold could not be calculated since hits and false alarms were zero during the calculation stages. In the 10 mm and 25 threshold categories, Off-MKF-WSM6 and Off-BMJ-KSL show the best forecasting abilities when considering the entire statistical indices.

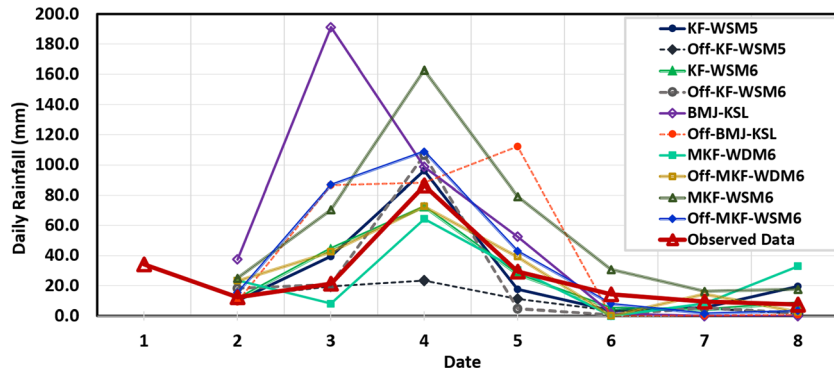


Figure 3. Area-averaged rainfall values.

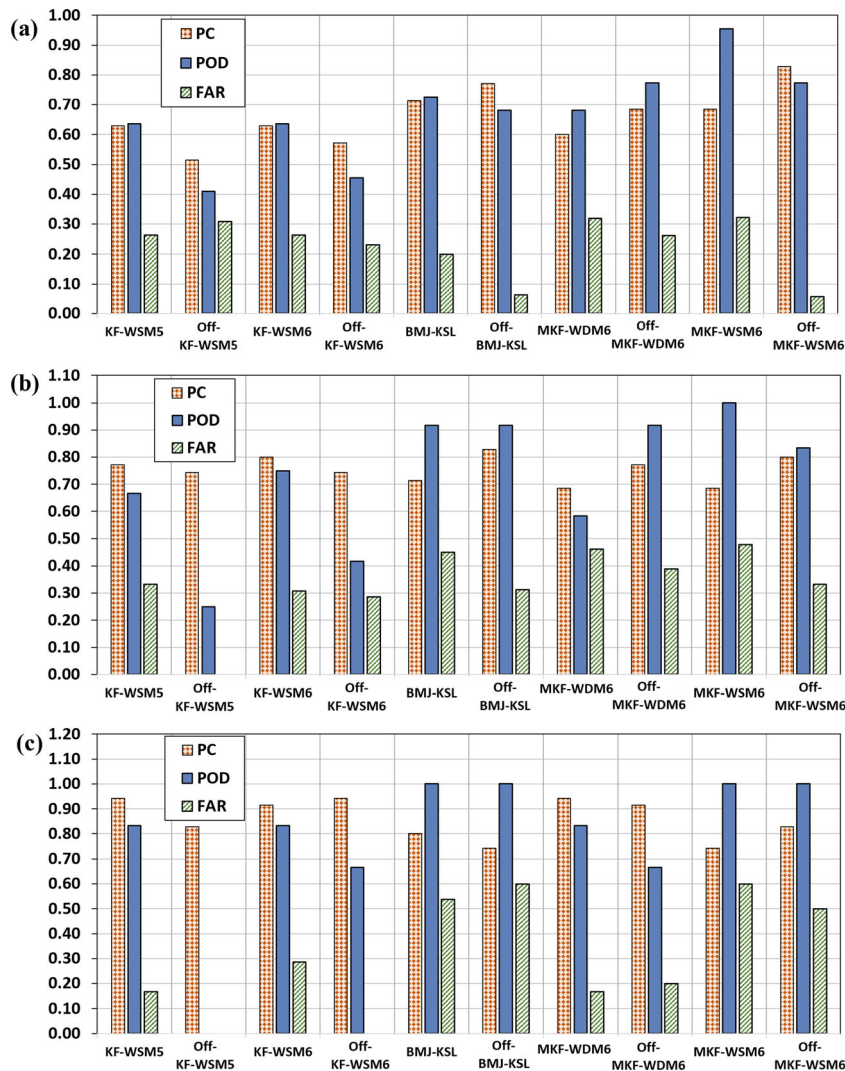


Figure 4. Statistical indices for (a) 10 mm limit; (b) 25 mm limit; and (c) 50 mm limit. The x-axis represents the combination reference number.

In general, Off-KF-WSM6 and MKF-WDM6 combination results in the highest threshold category are superior.

Figure 5 depicts the averaged ETS and bias (B) values calculated from the results of the three threshold classes, and turning off the CPS in the

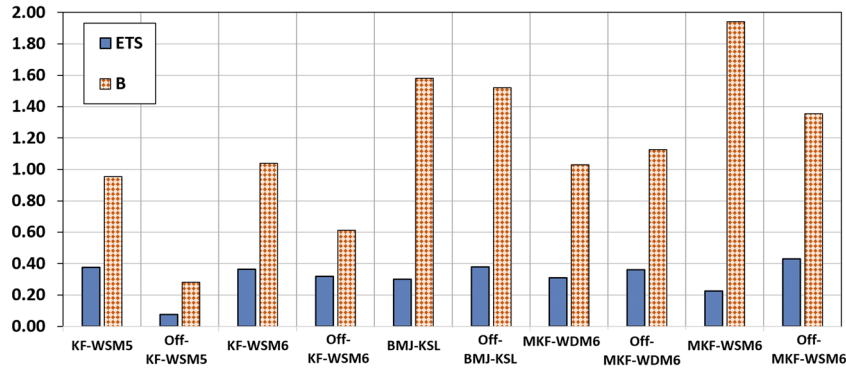


Figure 5. Averaged ETS and bias (B) for three limits.

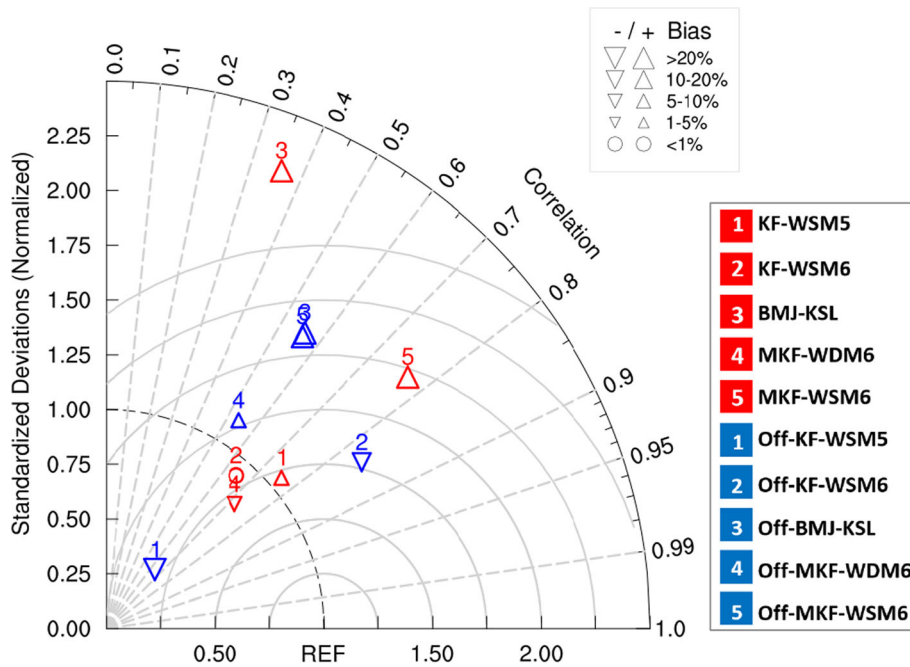


Figure 6. Normalised Taylor diagram results.

innermost domain (D3) yields mixed results among the tested cases analysed. Pursuant to the ETS metrics, only combinations with the BMJ and MKF schemes demonstrate an increase in their cumulus scheme-off configurations, while the KF scheme exhibits a decline. Except for the MKF-WDM6 combination, almost all investigated combinations have lower bias values after disabling the CPS in their innermost domain, implying improved bias metrics. So, when the outcomes from ETS and the Bias metrics are combined, the combinations that show improvement on both metrics after turning off the CPS in the innermost domain are BMJ-KSL and MKF-WSM6, whereas Off-MKF-WSM6 has the highest ETS value (0.43).

Moreover, Off-MKF-WSM6, KF-WSM5, and KF-WSM6 have better overall performances,

according to figure 5. Concerning the prediction of different rainfall intensities among these three best combinations (KF-WSM5, KF-WSM6, Off-MKF-WSM6), KF-WSM5 demonstrates the best capability in reproducing heavy rainfall intensity (50 mm threshold), whereas Off-MKF-WSM6 exhibits the best capability in regenerating light rainfall intensity (10 mm threshold).

3.2 Continuous verification method comparison – normalised Taylor diagram

Figure 6 graphically depicts the results relevant to the normalised Taylor diagram. The KF-WSM5, KF-WSM6 and MKF-WDM6 models have correlation coefficients above 0.60 and the lowest remaining parameter values. They are close to

the dashed arc in this Taylor diagram and generally agree well with the observation data. Even though Off-KF-WSM6 does have the highest correlation, it differs more from the observed precipitation values than KF-WSM6. Although BMJ-KSL and MKF-WSM6 have normalised standard deviation values greater than 1.6, MKF-WSM6 exhibits noticeably higher correlation (correlation value is 0.77) and lower NRMSE value (NRMSE value is 1.20) compared to the cumulus scheme off domains setup. When considering overall performances, the ability to predict rainfall was not improved by turning off the cumulus scheme in the finer domain.

3.3 Continuous verification method comparison – spatiotemporal analysis

The results of the spatiotemporal analysis for the day with the most rainfall (04/12/2019) are shown in figure 7. In each diagram, the grid-wise correctly predicted area (GCPA) is indicated to facilitate the spatiotemporal evaluation. According to the computed GCPA values, the KF-WSM5 and MKF-WDM6 models significantly degrade their performance in the tested cumulus scheme-off configuration, but the BMJ-KSL and MKF-WSM6 models exhibit conflicting behaviour. Off-BMJ-KSL has the highest GCPA (GCPA value is 97.7%).

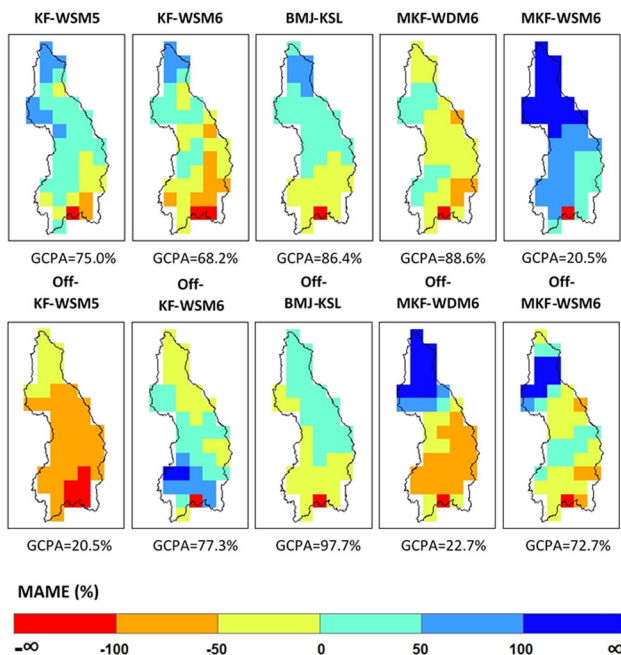


Figure 7. Spatial distribution of WRF model results on 04/12/2019.

Furthermore, the tested cumulus scheme off setup does not show an overly improved KF-WSM6 model. However, when the cumulus scheme is disabled inside its finer domain, the MKF-WSM6 model shows a notable improvement. Off-KF-WSM5 spatially underestimates the rainfall, while MKF-WSM6 spatially overestimates it.

3.4 Summary of results

The acquired categorical verification results are consistent with the work of Jeworrek *et al.* (2019) and Han and Hong (2018), which implies that turning off the CPS may enhance the rainfall forecast. As shown in table 2, in the cumulus scheme-off configuration, four of the five combinations (excluding MKF-WDM6) exhibit improvement in bias metrics, while three (except combinations with the KF scheme) demonstrate advancement in ETS metrics. It should also be highlighted that 3-km resolution in the innermost domain (D3) may still be insufficient to explicitly explain the convection that triggers rainfall in the basin. Moreover, the inclusion of solely the highest recorded precipitation day (December 4, 2019) in the present investigation does not yield any alterations to the current key findings of the categorical verification analysis (not shown).

However, analysis of the results in figure 6 pertaining to the normalised Taylor diagram suggests that deactivating the cumulus scheme does not significantly enhance predicting skill (see table 2). Cumulus is disabled for the innermost domain (D3) in the cumulus scheme off configuration. Hence it is possible that the setting could conceivably emanate from the outer domain (D2). Cumulus scheme-off configurations prevent precipitation rapidly because the temperature and humidity flow from the radiation physics and boundary layer physics schemes can significantly influence the grid-wise temperature distribution patterns and mixing conditions. This result is in line with other research investigations conducted by Sun and Barros (2014) and Lee *et al.* (2011).

According to the results of the comparative spatial analysis in table 2, the BMJ-KSL combination with activating and deactivating configurations is the most effective. The BMJ is a moist adjustment parameterization that was created for the convective clouds and posited that the temperature and moisture profiles in a column with enough resolved-scale vertical motion and

Table 2. *Statistical indices related to evaluated methods. Bold values indicate the first three highest performed combinations in each statistical indices category.*

Combination	Categorical verification		Taylor diagram			Spatial distribution
	ETS	B	<i>r</i>	NSD	NRMSE	GCPA (%)
KF-WSM5	0.38	0.95	0.76	1.06	0.72	75.0
Off-KF-WSM5	0.08	0.28	0.64	0.35	0.82	20.5
KF-WSM6	0.36	1.04	0.65	0.92	0.81	68.2
Off-KF-WSM6	0.32	0.61	0.84	1.40	0.78	77.3
BMJ-KSL	0.30	1.58	0.36	2.24	2.20	86.4
Off-BMJ-KSL	0.38	1.52	0.56	1.63	1.36	97.7
MKF-WDM6	0.31	1.03	0.72	0.82	0.71	88.6
Off-MKF-WDM6	0.36	1.13	0.54	1.13	1.03	22.7
MKF-WSM6	0.22	1.94	0.77	1.80	1.20	20.5
Off-MKF-WSM6	0.43	1.36	0.56	1.61	1.31	72.7

instability are instantly relaxed toward observed neutral structures (Betts and Miller 1986). In earlier investigations, the BMJ scheme has been found to more closely match the ground truth observations in the spatiotemporal evaluations compared with the other CPSs (Ratna *et al.* 2014; Remesan *et al.* 2015). In this evaluation, the BMJ scheme performs well with the KSL scheme despite the fact that it does not clearly define the upward and downward movements of the air current at subgrid scales. The KSL scheme utilises a lower limit during the condensation, leading to rapid precipitation that increases total precipitation and shifts downpours upstream (Mielikainen *et al.* 2013).

The variations in topography or circulation across the catchment are not taken into account during the spatiotemporal analysis in ArcGIS with the inverse distance weighting (IDW) technique tool. In contrast to the spatiotemporal analysis results, the 2 × 2 contingency table and normalised Taylor diagram results were therefore discussed in greater detail (see table 2 and figure 6).

The model combinations that use the KF cumulus scheme produce the best performances in this research. This assertion is consistent with the findings of Pennelly *et al.* (2014), who used five alternative cumulus schemes for three flooding events in Alberta, Canada, at a grid resolution of 15 km over three summer events. However, this scheme exhibits poor scores in spatiotemporal analysis across the catchment when combined with other physics. A similar finding was discovered by Gallus Jr (1999) during his spatial evaluation, and he also reported that greater rainfall rates are simulated with the higher model grid resolutions,

and the highest recorded rainfall is displaced by a great distance.

The KF-WSM5 combination is the best overall since it records excellent statistical indicators for the northeast extreme rainfall event modelled and tested over the catchment, among other combinations. Explicit feedback from the KF parameterization to mesoscale processes include temperature convection, mixing ratio of water vapour, and a wide variety of hydrometeors (Kuell *et al.* 2007). The KF trigger mechanism may be connected to the area of intensely heavy rainfall over the Badulu Oya watershed. Its trigger function mostly depends on the convective accessible potential energy (CAPE). As long as there is CAPE present, the convection will continue to take place. The thermodynamic characteristics and impacts of clouds are simulated using a cloud model when the KF scheme is triggered. This process permits modest amounts of heat and water vapour to be entrained into the updraft, which increases precipitation production (Kain and Fritsch 1990). Perhaps due to its interaction with the microphysics parameterization, the KF method also impacted the distribution and intensity of explicit precipitation. In general, WSM6 outperformed WSM5 (Kar and Tiwari 2016). Except for graupel, five water continuity equations in the WSM5 may be solved by the WSM6. Even if a graupel particle was added to the WSM5 scheme to make it more complicated, its performance in this investigation was still inferior to that of the WSM5 with KF combination. Similar to the outcome reported by Akinola and Yin (2019) across the southern portion of Nigeria, WSM6’s inability to anticipate heavy rainfall may be due to the slowdown in condensation.

Additionally, Off-MKF-WSM6 and MKF-WDM6 combinations based on the MKF cumulus scheme performed well during the evaluations. According to Zheng *et al.* (2016), the MKF scheme could perform better for greater resolution ground rainfall forecasts, which is consistent with the aforementioned remark. This scheme takes into account the subgrid-scale cloud-radiation interaction, the impact of convective cloud vertical profiles, and the saturation level of a parcel. In this investigation, the KF scheme was superior to the BMJ scheme. Bukovsky and Karoly (2009) reported similar results after evaluating a few numbers of physics combinations in the WRF-ARW model, including such two cumulus schemes and land surface schemes, for four months at 30 km across the United States.

Different cumulus and microphysics parameterizations and cumulus scheme activation circumstances may result in studies with noticeable variations. This makes it challenging to select the experiment with the best performance. Furthermore, this study utilises the same physics option in each domain rather than assessing the effect of altering different physics schemes in each domain, particularly in the innermost domain. According to Dudhia (2014), model outputs can differ when using alternative parameterization schemes in available domains. Consequently, the research requires further instances to investigate the statistical implications.

4. Conclusions

An assessment of cumulus parameterization conditions and physical parameterization schemes of the WRF-ARW model was carried out for an extreme northeast monsoon event over the Badulu Oya Basin, Sri Lanka. The results revealed susceptibility to the verification method, whether it was a continuous or categorical verification method.

The statistical measures produced from this case study make it very evident that KF experiments are the most effective. Additionally, the skill is not enhanced by deactivating this scheme for the 3 km resolution domain. This assertion is substantiated by higher values of ETS and correlation in the categorical verification approach and in the Taylor diagram method, respectively, when activation of the KF scheme in the finer domain is compared to its counterpart. Furthermore, in the spatial

analysis, the KF-WSM5 combination exhibits a noticeable decline in performance, defined by the GCPA value, when the cumulus-off setup is utilised. As a result, there was no added benefit from turning off the KF scheme at this resolution. More studies are required to find out how sensitive this cumulus scheme is to the domain integration resolution.

The KF experiment utilising the WSM5 microphysics scheme was selected as the most appropriate combination out of all the parameterized cumulus experiments, improving one's ability to depict the extreme northeast monsoon precipitation event generated in the case study. The KF scheme's feedback improved and preconditioned the environment, enabling a relatively accurate portrayal of the isolated convective cells and the precipitation that resulted from them.

Despite the complexity of the WSM6 system with the KF scheme, it was found that the WSM5 scheme, which employed the rime ice particles, was able to recreate the accumulated surface rainfall more accurately. Particles of dense rime ice called graupel make up WSM6. The presence of the graupel as a further forecasting parameter in the WSM5 scheme makes the WSM6 more sophisticated. The inability of WSM6 to predict severe rainfall in this study could be attributed to the slowness of condensation.

Overall, this study evaluated how the WRF represented the extreme rainfall event that occurred from 1 to 8 December 2019 during the northeast monsoon over Badulla, Sri Lanka, and determined a physics scheme combination that more accurately describes this particular event. Ultimately, it was determined that the KF-WSM5 experiment performed the best in this instance. Additionally, the KF cumulus parameterization should be used for domain resolutions of 3 km since higher skill was discovered when activating this cumulus scheme at this resolution. The representation of extreme precipitation events in Sri Lanka should be improved further by future research that examines the physical mechanisms within these combinations and identifies adjustments connected to the selected domain resolutions in these schemes.

Acknowledgements

The authors acknowledge the University of Peradeniya Computer Department for providing the

High-Performance Computing (HPC) resources to conduct the research simulations. The Department of Meteorology, Sri Lanka (DMSL), also deserves praise for supplying the authors with recorded precipitation data for the duration of the research.

Author statement

PGSG: Conceptualisation, methodology, simulations, formal analysis, writing – original draft, review and editing; PN: Supervision, conceptualisation, resources, review and editing; RAA: Supervision, review and editing.

References

- Akinola O E and Yin Y 2019 An assessment of the role of ice hydrometeor-types in WRF bulk microphysical schemes in simulating two heavy rainfall events over southern Nigeria; *Atmosphere* **10(9)** 513, <https://doi.org/10.3390/atmos10090513>.
- Arakawa A 2004 The cumulus parameterization problem: Past, present, and future; *J. Clim.* **17(3)** 2493–2525, [https://doi.org/10.1175/1520-0442\(2004\)017%3c2493:ratcpp%3e2.0.co;2](https://doi.org/10.1175/1520-0442(2004)017%3c2493:ratcpp%3e2.0.co;2).
- Arianti I, Soemarno, Hasyim A W and Sulistyono R 2018 Rainfall estimation by using Thiessen polygons, Inverse Distance Weighted, Spline, and Kriging methods: A case study in Pontianak, West Kalimantan; *Int. J. Educ. Res.* **6(11)** 693–709, <https://www.ijern.com/journal/2018/November-2018/25.pdf>.
- Atukorala A K D N 2012 Diversion of excess water in Badulu Oya for augmentation of Loggal Oya reservoir for generation of hydropower (concept paper); *ENGINEER* **45(03)** 45–48, <https://doi.org/10.4038/engineer.v45i3.6942>.
- Avolio E and Federico S 2018 WRF simulations for a heavy rainfall event in southern Italy: Verification and sensitivity tests; *Atmos. Res.* **209** 14–35, <https://doi.org/10.1016/j.atmosres.2018.03.009>.
- Balachandran S, Geetha B, Ramesh K, Deepa R V, Mourya Y P and Rakhil K S 2020 *Report on Northeast Monsoon – 2019 (IMD Chennai Scientific Report No. IMDC-SR/08)* Chennai: Regional Meteorological Centre, Chennai, https://mausam.imd.gov.in/chennai/mcdata/ne_monsoon_2019.pdf.
- Bandurathna L B, Wang L, Zhou X, Cheng Y and Chen L 2021 Intraseasonal oscillation of the southwest monsoon over Sri Lanka and evaluation of its subseasonal forecast skill; *Atmos. Ocean. Sci. Lett.* **14(6)** 100062, <https://doi.org/10.1016/j.aosl.2021.100062>.
- Betts A K and Miller M J 1986 A new convective adjustment scheme. Part II: Single column tests using GATE wave, BOMEX, ATEX and arctic air-mass data sets; *Quart. J. Roy. Meteorol. Soc.* **112(473)** 693–709, <https://doi.org/10.1256/smsqj.47307>.
- Bliznak V, Kaspar M, Muller M and Zacharov P 2019 Sub-daily temporal reconstruction of extreme precipitation events using NWP model simulations; *Atmos. Res.* **224** 65–80, <https://doi.org/10.1016/j.atmosres.2019.03.019>.
- Brown B, Atger F, Brooks H, Casati B, Damrath U, Ebert B, Ghelli A, Nurmi P, Stephenson D, Wilson C and Wilson L 2004 *Recommendations for the verification and intercomparison of QPFs from operational NWP models (WWRP/WGNE Joint Working Group on Verification)*, Centre for Australian Weather and Climate Research, Australia, https://www.cawcr.gov.au/projects/verification/WGNE/QPF_verif_recomm.pdf.
- Bruno F, Cocchi D, Greco F and Scardovi E 2014 Spatial reconstruction of rainfall fields from rain gauge and radar data; *Stoch. Environ. Res. Risk. Assess.* **28(5)** 1235–1245, <https://doi.org/10.1007/s00477-013-0812-0>.
- Bryan G H and Morrison H 2012 Sensitivity of a simulated squall line to horizontal resolution and parameterization of microphysics; *Mon. Wea. Rev.* **140(1)** 202–225, <https://doi.org/10.1175/mwr-d-11-00046.1>.
- Bukovsky M S and Karoly D J 2009 Precipitation simulations using WRF as a nested regional climate model; *J. Appl. Meteorol. Climatol.* **48(10)** 2152–2159, <https://doi.org/10.1175/2009jamc2186.1>.
- Chawla I, Osuri K K, Mujumdar P P and Niyogi D 2018 Assessment of the Weather Research and Forecasting (WRF) model for simulation of extreme rainfall events in the upper Ganga Basin; *Hydrol. Earth Syst. Sci.* **22(2)** 1095–1117, <https://doi.org/10.5194/hess-22-1095-2018>.
- Clark A J, Kain J S, Marsh P T, Correia Jr J, Xue M and Kong F 2012 Forecasting tornado pathlengths using a three-dimensional object identification algorithm applied to convection-allowing forecasts; *Wea. Forecasting* **27(5)** 1090–1113, <https://doi.org/10.1175/waf-d-11-00147.1>.
- Darshika D W T T and Premalal K H M S 2015 Simulate heavy rainfall during 19th to 28th December 2014 using WRF for different atmospheric physics; *Sri Lanka J. Meteorol.* **1** 32–40, https://meteo.gov.lk/images/sljom/thanuja_ab.pdf.
- Dasari H P and Salgado R 2015 Numerical modelling of heavy rainfall event over Madeira Island in Portugal: Sensitivity to different micro physical processes; *Meteorol. Appl.* **22(1)** 113–127, <https://doi.org/10.1002/met.1375>.
- De Meij A, Vinuesa J F and Maupas V 2018 GHI calculation sensitivity on microphysics, land-and cumulus parameterization in WRF over the Reunion Island; *Atmos. Res.* **204** 12–20, <https://doi.org/10.1016/j.atmosres.2018.01.008>.
- DMSL 2020 *Department of Meteorology, Sri Lanka*, <http://www.meteo.gov.lk/index.php?lang=en>.
- Donner L J, Seman C J, Hemler R S and Fan S 2001 A cumulus parameterization including mass fluxes, convective vertical velocities, and mesoscale effects: Thermodynamic and hydrological aspects in a general circulation model; *J. Clim.* **14(16)** 3444–3463, [https://doi.org/10.1175/1520-0442\(2001\)014%3c3444:acpimf%3e2.0.co;2](https://doi.org/10.1175/1520-0442(2001)014%3c3444:acpimf%3e2.0.co;2).
- Dudhia J 1989 Numerical study of convection observed during the winter monsoon experiment using a mesoscale two-dimensional model; *J. Atmos. Sci.* **46(20)** 3077–3107, [https://doi.org/10.1175/1520-0469\(1989\)046%3c3077:msocod%3e2.0.co;2](https://doi.org/10.1175/1520-0469(1989)046%3c3077:msocod%3e2.0.co;2).
- Dudhia J 2014 *Overview of WRF physics*; Boulder: University Corporation for Atmospheric Research, Colorado, http://www2.mmm.ucar.edu/wrf/users/tutorial/201401/Physics_full.pdf.

- Emanuel K A 1991 A scheme for representing cumulus convection in large-scale models; *J. Atmos. Sci.* **48**(21) 2313–2329, [https://doi.org/10.1175/1520-0469\(1991\)048%3C2313:asfrcc%3E2.0.co;2](https://doi.org/10.1175/1520-0469(1991)048%3C2313:asfrcc%3E2.0.co;2).
- Gallus Jr W A 1999 Eta simulations of three extreme precipitation events: Sensitivity to resolution and convective parameterization; *Wea. Forecasting* **14**(3) 405–426, [https://doi.org/10.1175/1520-0434\(1999\)014%3c0405:esotep%3e2.0.co;2](https://doi.org/10.1175/1520-0434(1999)014%3c0405:esotep%3e2.0.co;2).
- Government of Sri Lanka, World Food Programme 2019 *Summary Situation Update of Heavy Rain and Flooding (03 December 2019)*; Colombo: United Nations Office for the Coordination of Humanitarian Affairs (OCHA), <https://reliefweb.int/report/sri-lanka/sri-lanka-summary-situation-update-heavy-rain-and-flooding-03-december-2019>.
- Han J Y and Hong S Y 2018 Precipitation forecast experiments using the Weather Research and Forecasting (WRF) Model at gray-zone resolutions; *Wea. Forecasting* **33**(6) 1605–1616, <https://doi.org/10.1175/waf-d-18-0026.1>.
- Hasan M A and Islam A K M 2018 Evaluation of microphysics and cumulus schemes of WRF for forecasting of heavy monsoon rainfall over the southeastern hilly region of Bangladesh; *Pure Appl. Geophys.* **175**(12) 4537–4566, <https://doi.org/10.1007/s00024-018-1876-z>.
- Hong S Y and Dudhia J 2012 Next-generation numerical weather prediction: Bridging parameterization, explicit clouds, and large eddies; *Bull. Am. Meteorol. Soc.* **93**(1) ES6–ES9, <https://doi.org/10.1175/2011bams3224.1>.
- Hong S Y and Lim J O J 2006 The WRF single-moment 6-class microphysics scheme (WSM6); *Asia-Pacific J. Atmos. Sci.* **42**(2) 129–151, https://www.researchgate.net/profile/song-you-hong/publication/331192569_hongan_dlim-jkms-2006/links/5c6b581f92851c1c9dea9d10/hongandlim-jkms-2006.pdf.
- Hong S Y, Noh Y and Dudhia J 2006 A new vertical diffusion package with an explicit treatment of entrainment processes; *Mon. Wea. Rev.* **134**(9) 2318–2341, <https://doi.org/10.1175/mwr3199.1>.
- Huang Y C and Wang P K 2017 The hydrometeor partitioning and microphysical processes over the Pacific Warm Pool in numerical modeling; *Atmos. Res.* **183** 308–321, <https://doi.org/10.1016/j.atmosres.2016.09.009>.
- Huang Y J, Cui X P and Wang Y P 2016 Cloud microphysical differences with precipitation intensity in a torrential rainfall event in Sichuan, China; *Atmos. Ocean. Sci. Lett.* **9**(2) 90–98, <https://doi.org/10.1080/16742834.2016.1139436>.
- Jeworrek J, West G and Stull R 2019 Evaluation of cumulus and microphysics parameterizations in WRF across the convective gray zone; *Wea. Forecasting* **34**(4) 1097–1115, <https://doi.org/10.1175/waf-d-18-0178.1>.
- Ji F, Ekstrom M, Evans J P and Teng J 2013 Evaluating rainfall patterns using physics scheme ensembles from a regional atmospheric model; *Theor. Appl. Climatol.* **115**(1–2) 297–304, <https://doi.org/10.1007/s00704-013-0904-2>.
- Jimenez P A, Dudhia J, Gonzalez-Rouco J F, Navarro J, Montavez J P and Garcia-Bustamante E 2012 A revised scheme for the WRF surface layer formulation; *Mon. Wea. Rev.* **140**(3) 898–918, <https://doi.org/10.1175/mwr-d-11-00056.1>.
- Kain J S 2004 The Kain–Fritsch convective parameterization: An update; *J. Appl. Meteorol.* **43**(1) 170–181, [https://doi.org/10.1175/1520-0450\(2004\)043%3c0170:tkcpau%3e2.0.co;2](https://doi.org/10.1175/1520-0450(2004)043%3c0170:tkcpau%3e2.0.co;2).
- Kain J S and Fritsch J M 1990 A one-dimensional entraining/detraining plume model and its application in convective parameterization; *J. Atmos. Sci.* **47**(23) 2784–2802, [https://doi.org/10.1175/1520-0469\(1990\)047%3c2784:aodepm%3e2.0.co;2](https://doi.org/10.1175/1520-0469(1990)047%3c2784:aodepm%3e2.0.co;2).
- Kar S C and Tiwari S 2016 Model simulations of heavy precipitation in Kashmir, India, in September 2014; *Nat. Hazards* **81**(1) 167–188, <https://doi.org/10.1007/s11069-015-2073-3>.
- Kueller V, Gassmann A and Bott A 2007 Towards a new hybrid cumulus parametrization scheme for use in non-hydrostatic weather prediction models; *Quart. J. Roy. Meteorol. Soc.* **133**(623) 479–490, <https://doi.org/10.1002/qj.28>.
- Kumar A, Dudhia J, Rotunno R, Niyogi D and Mohanty U C 2008 Analysis of the 26 July 2005 heavy rain event over Mumbai, India using the Weather Research and Forecasting (WRF) model; *Quart. J. Roy. Meteorol. Soc.* **134**(636) 1897–1910, <https://doi.org/10.1002/qj.325>.
- Kuo H L 1974 Further studies of the parameterization of the influence of cumulus convection on large-scale flow; *J. Atmos. Sci.* **31**(5) 1232–1240, [https://doi.org/10.1175/1520-0469\(1974\)031%3c1232:fsotpo%3e2.0.co;2](https://doi.org/10.1175/1520-0469(1974)031%3c1232:fsotpo%3e2.0.co;2).
- Kwon Y C and Hong S Y 2017 A mass-flux cumulus parameterization scheme across gray-zone resolutions; *Mon. Wea. Rev.* **145**(2) 583–598, <https://doi.org/10.1175/mwr-d-16-0034.1>.
- Lawrence D M and Webster P J 2002 The boreal summer intraseasonal oscillation: Relationship between northward and eastward movement of convection; *J. Atmos. Sci.* **59**(9) 1593–1606, [https://doi.org/10.1175/1520-0469\(2002\)059%3c1593:tbsior%3e2.0.co;2](https://doi.org/10.1175/1520-0469(2002)059%3c1593:tbsior%3e2.0.co;2).
- Lee S W, Lee D K and Chang D E 2011 Impact of horizontal resolution and cumulus parameterization scheme on the simulation of heavy rainfall events over the Korean Peninsula; *Adv. Atmos. Sci.* **28**(1) 1–15, <https://doi.org/10.1007/s00376-010-9217-x>.
- Lee J, Shin H H, Hong S Y, Jimenez P A, Dudhia J and Hong J 2015 Impacts of subgrid-scale orography parameterization on simulated surface layer wind and monsoonal precipitation in the high-resolution WRF model; *J. Geophys. Res.* **120**(2) 644–653, <https://doi.org/10.1002/2014jd022747>.
- Li F, Song J and Li X 2018 A preliminary evaluation of the necessity of using a cumulus parameterization scheme in high-resolution simulations of Typhoon Haiyan (2013); *Nat. Hazards* **92**(2) 647–671, <https://doi.org/10.1007/s11069-018-3218-y>.
- Lim J O J and Hong S Y 2005 Effects of bulk ice microphysics on the simulated monsoonal precipitation over East Asia; *J. Geophys. Res.* **110**(D24), <https://doi.org/10.1029/2005jd006166>.
- Lim K S S and Hong S Y 2010 Development of an effective double-moment cloud microphysics scheme with prognostic cloud condensation nuclei (CCN) for weather and climate models; *Mon. Wea. Rev.* **138**(5) 1587–1612, <https://doi.org/10.1175/2009mwr2968.1>.
- Liu D, Yang B, Zhang Y, Qian Y, Huang A, Zhou Y and Zhang L 2018 Combined impacts of convection and microphysics parameterizations on the simulations of

- precipitation and cloud properties over Asia; *Atmos. Res.* **212** 172–185, <https://doi.org/10.1016/j.atmosres.2018.05.017>.
- Lu G Y and Wong D W 2008 An adaptive inverse-distance weighting spatial interpolation technique; *Comput. Geosci.* **34(9)** 1044–1055, <https://doi.org/10.1016/j.cageo.2007.07.010>.
- Madhulatha A, Choi S J, Han J Y and Hong S Y 2021 Impact of different nesting methods on the simulation of a severe convective event over South Korea using the Weather Research and Forecasting Model; *J. Geophys. Res. Atmos.* **126(5)** 2020JD033084, <https://doi.org/10.1029/2020jd033084>.
- Maheskumar R S, Padmakumari B, Konwar M, Morwal S B and Deshpande C G 2018 Characterisation of hydrometeors and precipitation over the Indian monsoon region using aircraft measurements; *Atmos. Res.* **205** 147–154, <https://doi.org/10.1016/j.atmosres.2018.02.012>.
- McMillen J D and Steenburgh W J 2015 Impact of microphysics parameterizations on simulations of the 27 October 2010 Great Salt Lake–effect snowstorm; *Wea. Forecasting* **30(1)** 136–152, <https://doi.org/10.1175/waf-d-14-00060.1>.
- Mielikainen J, Huang B, Wang J and Huang H L A 2013 Compute unified device architecture (CUDA)-based parallelisation of WRF Kessler cloud microphysics scheme; *Comput. Geosci.* **52** 292–299, <https://doi.org/10.1016/j.cageo.2012.10.006>.
- Ministry of Defence 2019 *Situation Report Summary (Heavy rains, flooding, landslides), Sri Lanka, 1800 hours, 20-12-2019*; Colombo: Ministry of Defence, http://www.dmc.gov.lk/images/dmcreports/Situation_Summary_1800hrs_20122019edited3_1576862826.pdf.
- Mlawer E J, Taubman S J, Brown P D, Iacono M J and Clough S A 1997 Radiative transfer for inhomogeneous atmospheres: RRTM, a validated correlated-k model for the longwave; *J. Geophys. Res. Atmos.* **102(D14)** 16,663–16,682, <https://doi.org/10.1029/97jd00237>.
- Muhammadh K M, Mafas M M M and Weerakoon S B 2017 Rainfall forecast in the Upper Mahaweli basin in Sri Lanka using RegCM model; *J. Phys. Conf. Ser.* **822(1)** 012075, <https://doi.org/10.1088/1742-6596/822/1/012075>.
- Mukhopadhyay P, Taraphdar S, Goswami B N and Krishnakumar K 2010 Indian summer monsoon precipitation climatology in a high-resolution regional climate model: Impacts of convective parameterization on systematic biases; *Wea. Forecasting* **25(2)** 369–387, <https://doi.org/10.1175/2009waf2222320.1>.
- Mukul Tewari N C A R, Tewari M, Chen F, Wang W, Dudhia J, LeMone M A, Mitchell K, Ek M, Gayno G, Wegiel J and Cuenca R H 2004 Implementation and verification of the unified NOAA land surface model in the WRF model (Formerly Paper Number 17.5); *In 20th conference on weather analysis and forecasting/16th conference on numerical weather prediction* 11–15, https://ams.confex.com/ams/84Annual/techprogram/paper_69061.htm.
- Nandalal K D W, Sachindra D A and Ratnayake U R 2012 Application of WRF weather model to forecast precipitation in Nilwala river basin; *ENGINEER* **45(1)** 51–64, <https://doi.org/10.4038/engineer.v45i1.6949>.
- Nasrollahi N, AghaKouchak A, Li J, Gao X, Hsu K and Sorooshian S 2012 Assessing the impacts of different WRF precipitation physics in hurricane simulations; *Wea. Forecasting* **27(4)** 1003–1016, <https://doi.org/10.1175/waf-d-10-05000.1>.
- National Center for Atmospheric Research 2019 *WRF USERS PAGE*, https://www2.mmm.ucar.edu/wrf/users/namelist_best_prac_wps.html.
- National Center for Atmospheric Research 2020 *WRF USERS PAGE*, https://www2.mmm.ucar.edu/wrf/users/download_get_sources_wps_geog.html.
- NCAR 2019 *NCL*, <https://www.ncl.ucar.edu/index.shtml>.
- On N, Kim H M and Kim S 2018 Effects of resolution, cumulus parameterization scheme, and probability forecasting on precipitation forecasts in a high-resolution limited-area ensemble prediction system; *Asia-Pacific J. Atmos. Sci.* **54(4)** 623–637, <https://doi.org/10.1007/s13143-018-0081-4>.
- Pennelly C, Reuter G and Flesch T 2014 Verification of the WRF model for simulating heavy precipitation in Alberta; *Atmos. Res.* **135** 172–192, <https://doi.org/10.1016/j.atmosres.2013.09.004>.
- Perera E N C, Jayawardana D T and Jayasinghe P 2017 A rainfall intensity-duration threshold for mass movement in Badulla, Sri Lanka; *J. Geosci. Environ. Prot.* **5** 135–152, <https://doi.org/10.4236/gep.2017.512010>.
- Rajapaksha R M G N, Dharmagunawardhane H A, Attanayake A M A N B and Rekha Nianthi K W 2020 Altitudinal and temporal variation of surface water quality: An assessment in Badulu Oya Catchment, Sri Lanka; *GSC Biol. Pharm. Sci.* **11(3)** 226–236, <https://doi.org/10.30574/gscbps.2020.11.3.0181>.
- Ratna S B, Ratnam J V, Behera S K, Rautenbach C D, Ndarana T, Takahashi K and Yamagata T 2014 Performance assessment of three convective parameterization schemes in WRF for downscaling summer rainfall over South Africa; *Clim. Dyn.* **42(11)** 2931–2953, <https://doi.org/10.1007/s00382-013-1918-2>.
- Remesan R, Bellerby T, Holman I and Frostick L 2015 WRF model sensitivity to choice of parameterization: A study of the ‘York Flood 1999’; *Theor. Appl. Climatol.* **122(1)** 229–247, <https://doi.org/10.1007/s00704-014-1282-0>.
- Rodrigo C, Kim S and Jung I H 2018 Sensitivity study of WRF numerical modeling for forecasting heavy rainfall in Sri Lanka; *Atmosphere* **9(10)** 378, <https://doi.org/10.3390/atmos9100378>.
- Ruwangika A M, Perera A and Rathnayake U 2020 Comparison of Statistical, Graphical, and Wavelet Transform Analyses for Rainfall Trends and Patterns in Badulu Oya Catchment, Sri Lanka; *Complexity* **2020** 1–13, <https://doi.org/10.1155/2020/7146593>.
- Samarasingha S M T C, Sandaruwan M S, Sampath D S and Neluwala N G P B 2021 Dynamic downscaling of rainfall data for Deduru Oya River Basin using WRF weather model; *ENGINEER* **54(02)** 69–75, <https://doi.org/10.4038/engineer.v54i2.7443>.
- Scaff L, Prein A F, Li Y, Liu C, Rasmussen R and Ikeda K 2020 Simulating the convective precipitation diurnal cycle in North America’s current and future climate; *Clim. Dyn.* **55(1)** 369–382, <https://doi.org/10.1007/s00382-019-04754-9>.
- Schwartz C S and Liu Z 2014 Convection-permitting forecasts initialised with continuously cycling limited-area 3DVAR, ensemble Kalman filter, and “hybrid” variational–ensemble

- data assimilation systems; *Mon. Weather Rev.* **142**(2) 716–738, <https://doi.org/10.1175/mwr-d-13-00100.1>.
- Singh K S, Bonthu S, Purvaja R, Robin R S, Kannan B A M and Ramesh R 2018 Prediction of heavy rainfall over Chennai Metropolitan City, Tamil Nadu, India: Impact of microphysical parameterization schemes; *Atmos. Res.* **202** 219–234, <https://doi.org/10.1016/j.atmosres.2017.11.028>.
- Skamarock W C, Klemp J B, Dudhia J, Gill D O, Liu Z, Berner J, Wang W, Powers J G, Duda M G, Barker D M and Huang X Y 2019 A description of the advanced research WRF model version 4; *National Center for Atmospheric Research: Boulder, CO, USA* **145** 145, <https://opensky.ucar.edu/islandora/object/technotes:576/datastream/PDF/download/citation.pdf>.
- Staff Writer 2019 *News 1st.*, <https://www.newsfirst.lk/2019/12/22/heavy-rains-across-the-island-disrupts-lives/>.
- Sun X and Barros A P 2014 High-resolution simulation of tropical storm Ivan (2004) in the Southern Appalachians: Role of planetary boundary-layer schemes and cumulus parametrization; *Quart. J. Roy. Meteorol. Soc.* **140**(683) 1847–1865, <https://doi.org/10.1002/qj.2255>.
- Tian J, Liu J, Yan D, Li C and Yu F 2017 Numerical rainfall simulation with different spatial and temporal evenness by using a WRF multiphysics ensemble; *Nat. Hazards Earth Syst. Sci.* **17**(4) 563–579, <https://doi.org/10.5194/nhess-17-563-2017>.
- Vaidya S S and Singh S S 2000 Applying the Betts–Miller–Janjic scheme of convection in prediction of the Indian monsoon; *Weather Forecast.* **15**(3) 349–356, [https://doi.org/10.1175/1520-0434\(2000\)015%3c0349:atbmjs%3e2.0.co;2](https://doi.org/10.1175/1520-0434(2000)015%3c0349:atbmjs%3e2.0.co;2).
- Warner T T, Peterson R A and Treadon R E 1997 A tutorial on lateral boundary conditions as a basic and potentially serious limitation to regional numerical weather prediction; *Bull. Am. Meteorol. Soc.* **78**(11) 2599–2618, [https://doi.org/10.1175/1520-0477\(1997\)078%3c2599:atolbc%3e2.0.co;2](https://doi.org/10.1175/1520-0477(1997)078%3c2599:atolbc%3e2.0.co;2).
- Wilks D S 2011 *Statistical methods in the atmospheric sciences (Vol. 100)*; 3rd edn., USA: Academic Press.
- Yang B, Zhang Y and Qian Y 2012 Simulation of urban climate with high-resolution WRF model: A case study in Nanjing, China; *Asia-Pacific J. Atmos. Sci.* **48**(3) 227–241, <https://doi.org/10.1007/s13143-012-0023-5>.
- Zhang G J, Kiehl J T and Rasch P J 1998 Response of climate simulation to a new convective parameterization in the National Center for Atmospheric Research Community Climate Model (CCM3); *J. Clim.* **11**(8) 2097–2115, [https://doi.org/10.1175/1520-0442\(1998\)011%3c2097:rocsta%3e2.0.co;2](https://doi.org/10.1175/1520-0442(1998)011%3c2097:rocsta%3e2.0.co;2).
- Zheng Y, Alapaty K, Herwehe J A, Del Genio A D and Niyogi D 2016 Improving high-resolution weather forecasts using the Weather Research and Forecasting (WRF) Model with an updated Kain-Fritsch scheme; *Mon. Weather Rev.* **144**(3) 833–860, <https://doi.org/10.1175/mwr-d-15-0005.1>.

Corresponding editor: P A FRANCIS